

Critical angular momentum distributions in collapsars: quiescent periods from accretion state transitions in long gamma-ray bursts

Diego López-Cámara^{1,2}, William H. Lee² and Enrico Ramirez-Ruiz³

ABSTRACT

The rotation rate in pre-supernova cores is an important ingredient which can profoundly affect the post-collapse evolution and associated energy release in supernovae and long gamma ray bursts (LGRBs). Previous work has focused on whether the specific angular momentum is above or below the critical value required for the creation of a centrifugally supported disk around a black hole. Here, we explore the effect of the *distribution* of angular momentum with radius in the star, and show that qualitative transitions between high and low angular momentum flow, corresponding to high and low luminosity accretion states, can effectively be reflected in the energy output, leading to variability and the possibility of quiescent times in LGRBs.

Subject headings: accretion, accretion disks — gamma rays: bursts — hydrodynamics — supernovae: general

1. Introduction

The collapse of massive stellar cores producing Supernovae (SN) has been clearly linked to the production of Long Gamma Ray Bursts (LGRBs) in the last ten years (see Woosley & Bloom (2006); Gehrels, Ramirez-Ruiz & Fox (2009) for reviews), providing tantalizing clues to the progenitors and the environments in which they occur (Fruchter et al. 2006), as well as providing fresh glimpses of the high-redshift universe (e.g., Prochaska et al. 2009). A key ingredient in this context is the stellar rotation rate, impacting the energy release and general outcome of the event following the implosion of the Chandrasekhar-mass iron core.

¹Instituto de Ciencias Nucleares, UNAM, Apdo. Postal 70-543, México D.F. 04510, MEXICO

²Instituto de Astronomía, UNAM, Apdo. Postal 70-264, México D.F. 04510, MEXICO

³Department of Astronomy and Astrophysics, University of California, Santa Cruz, CA 95064, USA

Stellar evolution considerations have shown that it is non-trivial to have rapid rotation in the inner regions of the star, as mass loss and magnetic fields both conspire to reduce the pre-SN angular momentum. Calculations (Spruit 2002; Heger et al. 2005; Yoon & Langer 2005; Woosley & Heger 2006, hereafter WH06) indicate that the final distributions of specific angular momentum may not easily lead to the production of a centrifugally supported accretion disk following collapse, with the envelope experiencing essentially radial infall. This has generally been believed to be insufficient to power LGRBs since the lack of shocks and the associated dissipation are unable to transform gravitational binding energy into radiation effectively. A possible evolutionary channel that avoids some of the pitfalls associated with the giant phase was proposed in WH06 and by Yoon & Langer (2005), in which thorough mixing on the main sequence in very massive stars reduces mass and angular momentum losses. However, a large class of stars remains in which rotation will be substantially slowed in late evolutionary stages, thus influencing the outcome of the collapse.

The low angular momentum regime in collapsars has not been fully explored. In most cases, studies of the attending neutrino cooled accretion flows have considered specific rotation laws that guarantee by a large margin the formation of a centrifugally supported disk, either because the angular velocity is assumed to be nearly Keplerian, or because the absolute value of the angular momentum given implies a circularization radius much larger than the radius of the innermost stable circular orbit (ISCO), which in General Relativity is $r_{\text{ISCO}} = 3r_g$ for a Schwarzschild black hole, where M_{BH} is the black hole mass and $r_g = 2GM_{\text{BH}}/c^2$ (MacFadyen & Woosley 1999; Popham, Woosley & Fryer 1999; Heger et al. 2000; Narayan, Piran & Kumar 2001; Proga & Begelman 2003; Proga, MacFadyen, Armitage & Begelman 2003; Lee, Ramirez-Ruiz & Page 2005; Fujimoto et al. 2006; Nagataki et al. 2007). We previously studied (Lee & Ramirez-Ruiz 2006; López-Cámara et al. 2009, hereafter Paper I), cases at the threshold for disk formation, where a centrifugally supported disk gives way to nearly radial inflow due to relativistic effects, finding that even in the case of slow rotation, enough energy may be available through the formation of *dwarf* disks (Illarionov & Beloborodov 2001; Zalamea & Beloborodov 2009) in near free fall to power LGRBs. However, the distributions of specific angular momentum we considered were constant in the equatorial plane, and smoothly decreasing towards the rotation axis. This is unrealistic, as the specific angular momentum *increases* outwards in the core and envelope, with marked transitions at the boundaries between different layers in the star (see, e.g., Figure 2 in WH06).

Further, as the newborn black hole (BH) accretes infalling matter, both its mass and angular momentum increase, raising the threshold value of the critical angular momentum required for the formation of a centrifugally supported disk, $J_{\text{crit}} = 2r_g c$. The competition with the increase of angular momentum in the infalling material determines the large scale properties of the flow. This was recently pointed out and addressed by Janiuk & Proga

(2008) in simple form, generically by Kumar, Narayan & Johnson (2008a,b) in studying the effect of the distribution of angular momentum in the star on the light curve of LGRBs, and more recently by Lindner et al. (2010) in two-dimensional simulations of collapsar accretion.

In this study, we explore how different distributions of angular momentum as a function of radius, can have important effects on the qualitative properties of the accretion flow, and hence on the accretion rate and global energy release, which we quantify through the neutrino luminosity, L_ν . We pay particular attention to the general form and rate of increase of specific angular momentum with radius in the star in this respect, and show that state transitions may in principle produce observable consequences in LGRBs relevant to variability and periods of quiescence. In section § 2 we describe the assumptions and approximations made in our calculations and identify the numerical setup. Section § 3 is devoted to presenting the flow transitions which result from different angular momentum distributions, and § 4 to the conditions necessary for them to occur. In § 5 we combine these, given realistic angular momentum distributions, to investigate episodic energy release from accretion. Our conclusions and prospects for observability are discussed in § 6.

2. Setup and physics

The evolution of the infalling core and envelope after the formation of the central black hole from the stellar Iron core is followed with the same azimuthally symmetric, two dimensional Smooth Particle Hydrodynamics (SPH) code as in Paper I. The computational domain covers the region between spherical radii $R_{\text{in}} = 2 \times 10^6$ cm and $R_{\text{out}} = 2 \times 10^9$ cm, without assuming reflection symmetry with respect to the equatorial plane. The equation of state contains contributions to the total pressure P from an ideal gas of α particles and free nucleons in nuclear statistical equilibrium (NSE), P_{gas} , black-body radiation, P_{rad} , relativistic e^\pm pairs of arbitrary degeneracy, P_{e^\pm} (Blinnikov, Dunina-Barkovskaya & Nadyozhin 1996) and neutrinos. Neutronization, and a variable electron fraction are computed assuming charge neutrality and weak equilibrium (Beloborodov 2003; Lee, Ramirez-Ruiz & Page 2005), depending on whether the fluid is optically thin or thick to neutrinos. The neutrino emissivities which dominate the cooling arise from e^\pm capture onto free nucleons and e^\pm annihilation, and are computed from the tabulated results of Langanke & Martínez-Pinedo (2001) and the fitting functions of Itoh et al. (1996), respectively. A two-stream approximation including these processes, and coherent scattering off free nucleons was implemented to compute the local cooling rate (Popham & Narayan 1995; Di Matteo et al. 2002; Janiuk, Yuan, Perna & Di Matteo 2007). The neutrino luminosity L_ν is computed as the volume integral of the local neutrino emissivity, given the thermodynamical conditions present

(see eq.8 in Paper I). The equations of motion also include a full expression for the viscous stress tensor t_{ij} in azimuthal symmetry. We compute the coefficient of viscosity with the standard α prescription of Shakura & Sunyaev (1973), namely $\eta_v = \alpha \rho c_s H$, where c_s is the local sound speed, $H = c_s \Omega$ is the pressure scale height, and Ω is the local Keplerian orbital frequency. We have used $\alpha = 0.1$ throughout for the simulations described in this paper. Given that this form is only applicable if there is a rotating accretion structure, in the usual sense of largely centrifugal support with a additional pressure corrections, we use a switch (similar to that described by MacFadyen & Woosley (1999)) so the viscosity only operates when rotation dominates over essentially free infall. In practice this is carried out by comparing the local radial and azimuthal components of velocity, and allowing $\eta_v \neq 0$ only if $v_r/v_\phi \leq 1$ (the functional form is made continuous to avoid spurious transitional behavior when rotational support dominates).

As a generic initial condition we consider the 1D pre-supernova models of WH06. Specifically we used model 16TI, a rapidly rotating ($v_{\text{rot}} = 390 \text{ km s}^{-1}$), low metallicity ($Z = 0.01 Z_\odot$) WR star of $16 M_\odot$ with low mass loss ($2 M_\odot$ total loss up to the pre-supernova stage), with an Iron core of $M_{Fe} = 1.6 M_\odot$. This particular model did not consider the effects of internal magnetic fields. The density, temperature and radial velocity of the stellar core was mapped to two dimensions assuming spherical symmetry, while the Iron core was condensed onto a point mass at the origin representing the newly formed black hole and producing a pseudo-Newtonian potential according to the expression of Paczyński & Wiita (1980), $\phi = -GM_{\text{BH}}/(R - r_g)$. This reproduces the existence and location of the innermost stable circular orbit (ISCO) of the Schwarzschild solution in General Relativity, which is the leading effect in terms of separating the potential progenitors of GRBs into those which can eventually form a centrifugally supported accretion disk and those that cannot.

The distributions of specific angular momentum, \mathcal{J} in pre-supernova stars, as computed in evolutionary codes, generally follow a monotonic increase with radius, with sharp transitions at the interfaces between shells where the composition changes abruptly. Thus, to study the collapse, we separated the angular momentum distribution into radial and polar angle components as $\mathcal{J} = \mathcal{J}(R, \theta) = J(R)\Theta(\theta)$, where R is the spherical radius and θ is the polar angle, and assumed rigid body rotation on shells, with $\Theta(\theta) = \sin^2 \theta$. For the radial component, we considered various functional forms: a) linearly increasing with radius, $J(R) \propto R$; b) constant, $J(R) = J_0$ with one or more superimposed sharp increases, or spikes to mimic the transitions at shell boundaries; c) the distribution given in WH06 for model 16TI, multiplied by a normalization factor of order unity.

3. Flow transitions

3.1. Linear distributions of specific angular momentum.

In Paper I, we considered simple, constant distributions of $J(R)$ in order to gauge the effect of the absolute value of angular momentum and the general properties of the flow when compared to previous work, and provide a further guide. When $J(R) < J_{\text{crit}}$ no centrifugally supported disk formed, and as the black hole accreted matter and increased its mass, so did the value of J_{crit} , further inhibiting the creation of a disk. The energy released came from the equatorial compression of the infalling gas, with peak neutrino luminosities $L_\nu \simeq 10^{51} \text{ erg s}^{-1}$. On the other hand, when $J(R) \geq J_{\text{crit}}$, a hot shocked torus promptly formed, but the mass accretion rate onto the black hole, $\dot{M}_{\text{BH}} \sim 0.1\text{-}0.5M_\odot \text{ s}^{-1}$, was such that the equatorial angular momentum in the flow was always above J_{crit} , and the disk was never destroyed.

Given the general rising trend in the distribution of specific angular momentum in pre-SN models mentioned above, we first considered linearly increasing distributions in $J(R)$ by writing $J(R) = J_0 + m(R/R_{\text{out}})$ and computing cases with varying J_0 and m . For low ($J_0 \ll J_{\text{crit}}$) or high ($J_0 \gg J_{\text{crit}}$) values of the starting point in the distribution, and independently of the value of m , the result was akin to that previously obtained, namely, a quasi-radial inflow (QRI) or a long-lived accretion disk around the BH, respectively.

Intermediate cases, however, here when $0.85 \leq J_0/J_{\text{crit}} \leq 1.15$, exhibit diverse behavior depending on the rate of increase in $J(R)$, given by m . Setting $J_0/J_{\text{crit}} = 1.05$, for $m \simeq 2$, a centrifugally supported torus momentarily appears as the gas encounters the centrifugal barrier, and is subsequently accreted after a delay of $\simeq 0.1 \text{ s}$. This is simply a manifestation of the well-known “runaway radial” instability (Abramowicz, Calvani & Nobili 1983), triggered by the rapid rise in black hole mass and thus J_{crit} . Moreover, the short-lived disk is not able to perturb the upstream gas since the inflow is supersonic downstream of the shock front. Once the critical rotation rate rises above that of the angular momentum in the envelope, the gas is accreted essentially in a free fall time scale and the neutrino luminosity drops by about one order of magnitude, to $L_\nu \simeq 10^{51} \text{ erg s}^{-1}$. There is thus no “memory” in the flow, in the sense that once the transitory disk is destroyed, the subsequent material evolves as if the disk had never appeared. Figure 1 shows the neutrino luminosity L_ν for the cases where the angular momentum increases either rapidly (blue line), slowly (green line), or moderately (red solid line).

It is thus clear, as explored initially by Janiuk & Proga (2008), that the competition between the rise in angular momentum as one moves outward in the star, and the increase in BH mass, plays a fundamental role in the establishment of an accretion structure capable

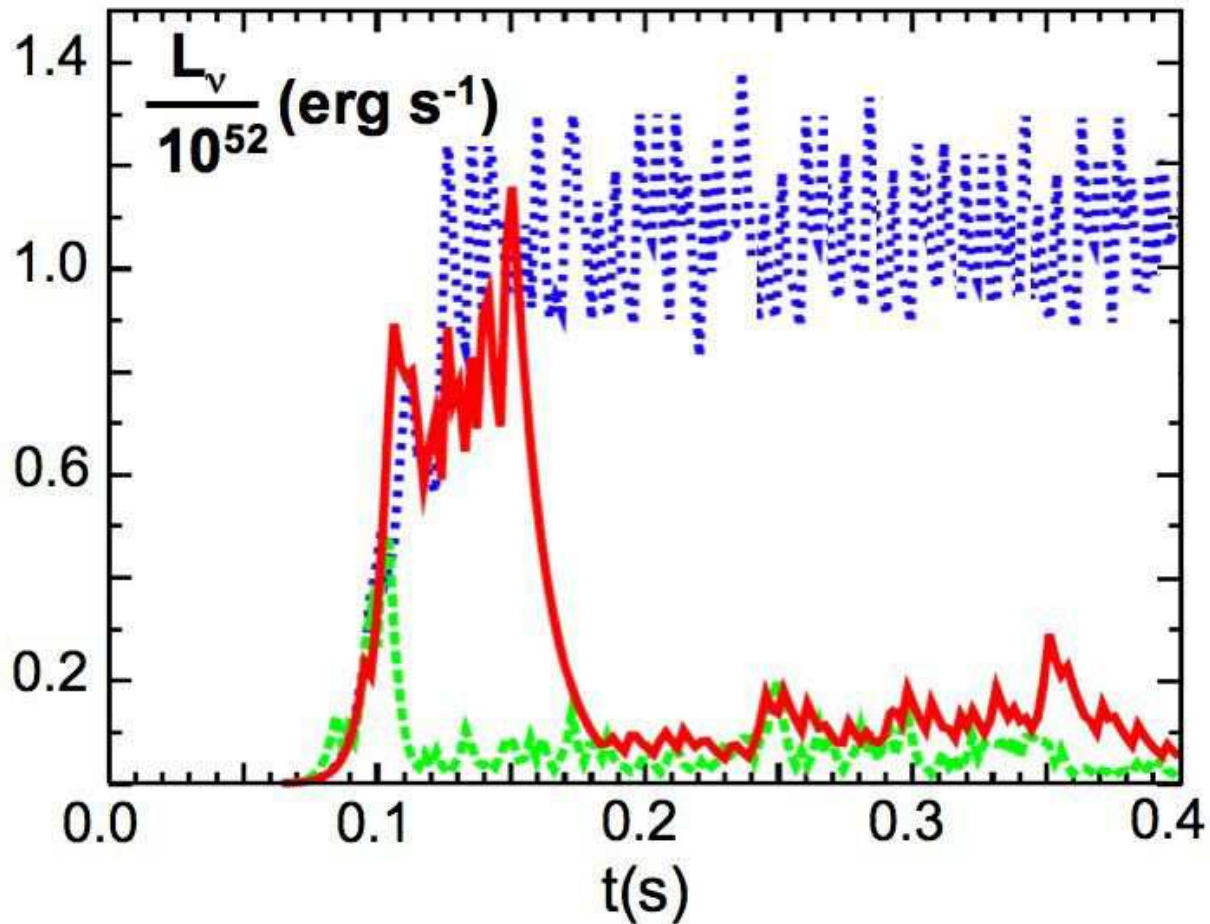


Fig. 1.— Neutrino luminosities (scaled to 10^{52} erg s^{-1}) for simulations with initially linear distributions of specific angular momentum, $J(R) = J_0 + mR/R_{\text{out}}$. The curves show the cases with $J_0/J_{\text{crit}} = 1.05$, for which the angular momentum increased rapidly (blue, $m = 3$, persistent disk); slowly (green, $m = 1$, no disk); and moderately (red, transitory disk correspondent to the critical value $m = 2$).

of releasing a significant amount of energy deep in the gravitational potential well. Furthermore, even a smooth, monotonically increasing distribution of $J(R)$, can produce temporal transitions between qualitatively different accretion states, namely, a QRI and a centrifugally supported disk.

3.2. Rapid transitions in the angular momentum distribution

The particular feature of strong jumps in $J(R)$ between neighboring shells found in stellar evolution calculations led us next to explore how such a qualitative variation in the angular momentum distribution can alter the properties of the accretion flow. For this, we considered a constant background distribution, with $J_0 \lesssim J_{\text{crit}}$, over which two radial shells where $J(R)$ reaches $1.5 J_{\text{crit}}$ are overlaid. Their width is $dR \simeq 5 \times 10^4$ cm, and they are separated by $\approx 2 dR$.

Since the angular momentum of the material initially reaching the BH is below the threshold for disk formation, a QRI promptly forms. Once the fluid in the rapidly rotating shells reaches the centrifugal barrier, this gives way to a shocked accretion disk, and both the accretion rate and neutrino luminosity rapidly rise (see Figure 2). The delay within which the disk forms is essentially the free fall time of the inner shell, $t_{\text{ff}} \propto \bar{\rho}^{-1/2} \sim 0.1$ s. In this simulated case, the inter-shell region contains enough material to completely overwhelm the first disk, leading to a second episode of QRI. This now lasts until the arrival of the second shell, with a delay again given by its proper free fall time. Even though the transitions are clearly visible in both the accretion rate and the luminosity, some differences clearly stand out. First, while \dot{M}_{BH} decreases by less than 30%, the luminosity drops by more than one order of magnitude. The discrepancy is due to the fundamental morphological change in the accretion flow: the QRI has a high mass accretion rate but an extremely low efficiency for converting gravitational potential energy into internal energy (it resembles Bondi accretion in this sense), while the centrifugally supported accretion disk allows for substantial energy conversion and dissipation, leading to higher luminosities. The associated accretion efficiencies through neutrinos, $\eta_{\nu, \text{acc}} = L_{\nu} / \dot{M}_{\text{BH}} c^2$ are in the expected range of (1-10)% for differentially rotating neutrino cooled disks (Di Matteo et al. 2002; Lee, Ramirez-Ruiz & Page 2005), and a factor of 10 or more below this for the QRI, where the emission is due to equatorial compression of the flow to a degree which depends on the value of the angular momentum used (Lee & Ramirez-Ruiz 2006, Paper I). Second, there is a slight delay in the correlated temporal variations of L_{ν} and \dot{M}_{BH} . Those in the former come slightly earlier, since the spikes in the accretion rate actually correspond to the mass accreted as the slowly rotating shells approach the black hole and the differentially rotating disk is destroyed.

The duration of each interval is dictated in this case by the initial radial position and extent of each shell and the corresponding free fall times. Since both shells here have the same radial extent and their initial radii are comparable, the associated intervals of activity are comparable. Variations in the form and normalization of the rotation rate as a function of radius thus impinge upon the duration of active periods and their relative power output.

We thus conclude that the presence of rapidly rotating shells in a slowly rotating back-

ground flow can lead to transitions between the QRI, low-luminosity and the disk, high-luminosity states, with delays that are correlated with the initial position and width of such shells. This is valid as long as the upper and lower limits in the distribution lie below and above the critical rotation rate for the existence of a centrifugal barrier. With this in mind, we can now address possible effects in GRB central engines in more realistic way, using the particular distributions found in WH06.

4. State transitions and evolutionary pathways

Before we directly analyze the behavior resulting from the evolutionary model of WH06, let us consider under which conditions an infalling shell can destroy a centrifugally supported disk.

Qualitatively, one would expect that the relative mass of successive collapsing regions should play a role in determining the outcome of the flow structure. The limits are easy to visualize, as a low mass shell with little or no rotation will likely only perturb an existing, massive centrifugally supported disk. Conversely, a massive flow in near free fall, due to its high ram pressure, will destroy the small pre-existing disk. So where does the transition between the two types of flow lie? To address this issue, we performed generic calculations (again with model 16TI), and included variations in angular momentum, so that the masses of successive shells with high ($J_{\text{high}} = 3r_g c$, leading to a first disk) and low ($J_{\text{low}} = 1.9r_g c$, leading to QRI) angular momentum were M_d and M_{QRI} , respectively. Their position and width were adjusted to explore a range in $\mu = M_d/M_{\text{QRI}}$ from 0.1-10. An outer shell with high rotation will lead invariably to the formation of a centrifugally supported disk at late times. Note that since we are always assuming rigid body rotation on shells through $\Theta(\theta)$, it is only the ratio of the masses that is relevant here.

For the parameters given above, we find that if $\mu \leq 1/3$, the low-angular momentum QRI fully destroys the pre-existing accretion disk on a dynamical time scale. Later, when the second shell with $J = J_{\text{high}}$ reaches the centrifugal barrier, a new disk is created, which persists as long as the inflow has sufficient rotation. This is illustrated in the upper panel of Figure 3, where the velocity field shows the flow morphology, and in particular the formation of shocks in the disk at various stages of the collapse. For this regime, after an initial QRI ($t = t_1$) before the initial shell with $J = J_{\text{high}}$ reaches the inner boundary, a centrifugally supported disk is created ($t = t_2$) and subsequently destroyed ($t = t_3$). The associated neutrino luminosity shown in the top panel of Figure 3 exhibits a high-state stage between two low-state episodes.

For $\mu \geq 1/3$, the initial disk is able to absorb the impact of the infalling shell and survive as a coherent structure. Thus, when the second shell with rapid rotation approaches it merely adds to the existing disk activity, and continues its evolution rather unperturbed (bottom panel in Figure 3). The light curve in this case shows continuous emission at the high state for $t > t_2$.

We note here that the absolute values of J_{high} and J_{low} represent an additional factor which can alter the resulting state transitions. Morphologically, the QRI resembles Bondi accretion, where technically $J_{\text{low}} = 0$, and it is certainly inefficient in terms of energy release. But even a rotation rate below the critical value can have non-negligible consequences when combined with a shell slightly above this threshold, and alter the determination of the critical mass ratio $\mu = M_{\text{d}}/M_{\text{QRI}}$ required for the transition to occur. In an attempt to quantify this effect, we carried out several additional simulations. In the first case, we used $\mu = 1/3$ and $J_{\text{high}} = 3r_{\text{g}}c$ as before, but set $J_{\text{low}} = 0$, thus forcing the more massive shell into strict radial infall. The interaction now resulted in the full destruction of the centrifugally supported accretion disk. In the second, we changed the mass ratio to $\mu = 1$ and used $J_{\text{high}} = 3r_{\text{g}}c$ and $J_{\text{low}} = 0$. This time, the centrifugally supported disk survived during the entire simulation.

A simple explanation of this trend can be given as follows. The critical angular momentum for the appearance of the centrifugal barrier is $J_{\text{crit}} = 2r_{\text{g}}c$, and we write $J_{\text{low}} = Ar_{\text{g}}c$, where A is a normalization parameter. Keeping $J_{\text{high}} = 3r_{\text{g}}c$ as in the above examples, and assuming the result after both shells have approached the black hole is a mixed configuration where the available angular momentum has been distributed into both components, the specific angular momentum is now J' . In order for the disk to survive, we must have $J' \geq J_{\text{crit}}$, which translates after a few lines of algebra into a condition on the masses as $M_{\text{d}} \geq (2 - A)M_{\text{QRI}}$, or $\mu \geq (2 - A)$. For $A = 1.9$, as used in our standard case, this implies $\mu \geq 1/10$, roughly consistent with the factor $\mu = 1/3$ found above. If $A = 0$, as now tested, this yields $\mu \geq 2$ as a condition for disk survival, i.e., it must be more massive in order to avoid destruction. In the first test described above, where J_{low} is drastically reduced, the outcome is as expected and the disk disappears. In the second, the rise in disk mass is able to offset the drop in J_{low} and the centrifugally supported disk persists. The fact that the normalization in mass does not strictly follow our simple analytical prescription is clearly due to an oversimplification of the dynamics, but it appears nonetheless to capture the essential aspect of the problem.

5. Critical distributions of angular momentum and episodic energy release

The distribution of specific angular momentum for representative models taken from WH06 is shown in Figure 4. They explored a large set of parameters, considering different initial zero age main sequence masses, $(12 - 35)M_{\odot}$, various initial rotation rates, $(1 - 14)r_{gc}$ in $J(R)$, initial metallicities, $(0.01 - 1)Z_{\odot}$, mass loss, and the effects of magnetic fields (see Table 1). The resulting distributions span slightly more than two orders of magnitude, and all cases clearly show the same qualitative behavior. The general background is that of a power law rise, segmented with sharp drops at the interfaces of the various layers in the star—for example, the first drop corresponds to the boundary between the iron core and the carbon-oxygen (CO) shell. The resulting layers, with varying degrees of rotation and mass, must necessarily interact with one another as they collapse onto the central object. As before, we chose model 16TI as our fiducial angular momentum distribution, J_{16TI} .

We are unable to follow the collapse of the outer regions of the core and envelope, covering the entire spatial and temporal range required in the present simulations. This is mostly due to our choice of location for the inner boundary, with which we are able to resolve the transition from a QRI to a rotationally supported disk at a few Schwarzschild radii. Nevertheless, the various time scale associated with the arrival of particular shells at the centrifugal barrier can be roughly estimated for these models as the free fall time, and the previous analysis of high and low-angular momentum shells extended to this regime, which we do in what follows. In reality, pressure support within the envelope is non-negligible, so the corresponding times and mass accretion rates are somewhat longer and lower, respectively (see also the discussion by MacFadyen & Woosley (1999) related to the latter). The calculations by Lindner et al. (2010) show that the transitions in flow morphology resulting from the structure of the progenitor can indeed be manifested at late times.

In Figure 5 we show $J(R)_{16TI}$ (green dotted line) and $J_{crit}(R)$ (black solid line), the

Table 1: Representative models from WH06.

Model	$M_{ZAMS}[M_{\odot}]$	$v_{rot}[\text{km s}^{-1}]$	$Z[Z_{\odot}]$	$M_{loss}[M_{\odot}]$	B-field
16TB	16	305	0.01	0.71	no
16TE	16	305	0.01	4.02	no
12ON	12	400	0.1	1.07	yes
16TI	16	390	0.01	2.0	no
12TJ	12	380	0.01	0.46	yes
35OA	35	380	0.1	0.6	yes
16OH	16	325	0.1	6.82	yes

critical distribution for the formation of a centrifugal barrier assuming all the matter at $r < R$ has been accreted by the black hole. It is clear that up to $R^* \sim 2 \times 10^9 \text{ cm}$, $J(R)_{16\text{TI}} \leq J_{\text{crit}}(R)$. Thus for this case, during the first ten seconds (which corresponds to the free fall time required for the material departing from R^* to reach the black hole), we would have a QRI, low-luminosity phase, as the one seen in the upper panel of Figure 3. Given the uncertainties in the normalization of $J(R)$ and the spread seen in Figure 4, we now introduce a multiplicative scaling factor of order unity f into $J(R)_{16\text{TI}}$ and compute the corresponding infall time scales. In fact, f may be tuned, for example so that the condition $\mu = 1/3$, discussed in § 4 is satisfied or not between the initial disk and the first shell with low angular momentum (red solid line in Figure 5, with $f = 2$). Typically, f is of order unity, although re-normalizing some models to have $\mu = 1/3$ requires substantial deviations from this value (see Table 2).

For a normalization leading to a distribution below that with $\mu = 1/3$, a centrifugally supported disk created from the material in the shell in region “I” in Figure 5 would be destroyed by the QRI produced by the shell labeled “II”, and finally be followed by a second stable disk from region “III”. Using the free fall times for the interfaces between regions I, II and III we find that after a one-second delay, an initially high-luminosity phase of 1.1 seconds would be followed by a quiescent period of $\simeq 4.2$ s before activity resumed. Note that the initial black hole with $1.6M_{\odot}$ is formed from material with $R \lesssim 2 \times 10^8 \text{ cm}$ (which includes the first large discontinuity in the rotation rate), so no variable energy output emerges from this region.

For vanishing mass of a centrifugally supported disk ($\mu \rightarrow 0$), the luminosity is only that of the QRI at a level $L_{\nu} \simeq 10^{51} \text{ erg s}^{-1}$ (Lee & Ramirez-Ruiz 2006; López-Cámara et al. 2009). As long as $0 < \mu < 1/3$ is satisfied, as in the case shown in Figure 3a, the low-angular momentum shell has greater mass than the centrifugally supported disk and a first high-luminosity transient followed by a quiescent period gradually appears, as seen in Figure 6. We note that their respective durations, t_{d} and t_{q} are *independent* of the assumed strength of viscous transport, as they are purely dynamical features. The initial episode lasts until the interface of the high and low-angular momentum material, at the edge of the CO shell, reaches the centrifugal barrier, $t_{\text{d}} \simeq t_{\text{ff}}(r_{\text{CO}})$. The end of the subsequent quiescent interval, t_{q} , corresponds to the infall time of the second shell of rapidly rotating gas (above the threshold for centrifugal support). The net result is that the sum between t_{d} and t_{q} varies slightly as a function of μ for a given initial mass configuration (Figure 6). The neutrino luminosity in the high state is $L_{\nu} \simeq 10^{52} \text{ erg s}^{-1}$. On the other hand, when the threshold value $\mu = 1/3$ is reached, the quiescent interval vanishes as abruptly as the associated flow morphology. For larger values, L_{ν} can in principle remain uninterruptedly at the high level as long as there is mass feeding the disk. While for the particular case shown here the quiescent period lasts

for a few seconds, depending on the initial conditions in the progenitor it can in principle be substantially longer, matching those observed in GRB events.

6. Discussion and prospects for observability

We wish to stress that while we have presented the neutrino luminosity as a measure of energy output, it is by no means the only one possible, and should be viewed here as a proxy for central engine activity, like the mass accretion rate with which it is very closely correlated. One could equally use \dot{M} (as long as it occurs in state where energy is dissipated efficiently), or the power output in magnetic outflows as a measure of the ability to drive relativistic outflows. Our numerical scheme is geared towards appropriate handling of thermodynamics and the associated neutrino emission, so it is natural to rely on these properties when making quantitative statements.

It is one thing to have a variation in the energy release close to the BH, and another to have it manifest itself in the light curve of a LGRB. Now, the minimum time required for activity to lead to high energy emission is about 2 s, the crossing time for a relativistic outflow originating in the inner regions to pierce the stellar envelope (see, e.g., MacFadyen & Woosley 1999; Aloy et al. 2000; MacFadyen et al. 2001; Aloy et al. 2002; Ramirez-Ruiz et al. 2002; Zhang et al. 2003). The crossing time is estimated here simply as $t_{\text{cross}} = R_{\text{env}}/(c/\sqrt{3})$. In Table 2, we present a summary of our results for the models shown in Figure 4 and Table 1, computed at the threshold where $\mu = 1/3$ and a quiescent period is marginally present.

After an initial delay (t_{delay}) between the onset of core collapse and the initial rise in neutrino luminosity, a first disk is active for an interval t_{d} , followed by quiescence and late disk creation. Only models with $t_{\text{d}} \geq t_{\text{cross}}$, in boldface in Table 2, are potentially observable as producing a quiescent period in the high-energy light curve under this scheme. Note that f is of order unity, but was scaled both to larger and smaller values in order to find a condition at the threshold value, $\mu = 1/3$.

The most obvious limitation of the current study is the range of time scales directly modeled. Nevertheless, we believe the current analysis to be of relevance to the generic behavior in collapsing cores. Within this range, the current calculations clearly show that the characteristics of the energy output are closely correlated to the distribution of specific angular momentum in the progenitor star. The state transitions are abrupt, with the luminosity rising or dropping by more than one order of magnitude, and reflect the naturally short (ms) time scales in the vicinity of the accretor. The scaling to larger radii and longer time scales can lead to quiescent period such as those studied by Ramirez-Ruiz & Merloni (2001), which

in this case would be related to dormant periods in the central engine (Ramirez-Ruiz et al. 2001). Ramirez-Ruiz & Merloni (2001) found that a small fraction, $\simeq 15\%$, of long GRBs exhibit at least one quiescent interval, with about one quarter of these showing two such episodes. Furthermore, the durations of the quiescent and subsequent period of activity were found to be directly correlated. We believe it is possible to account generically for this behavior under the present picture in at least two relevant aspects.

First, the number of shell-like jumps in the distribution of angular momentum within the star is small (one or two), accounting roughly for the number of transitions observed. The second point is related to the correlation itself. A short quiescent interval arises when the low-angular momentum shell has a narrow radial extent. Its inner limit at r_1 is fixed by the transition at the edge of the CO core and remains approximately at the same radius, independently of the normalization of angular momentum through the parameter f . The outer boundary at r_2 on the other hand, varies with f (see Figure 5). Due to the latter and to the fact that J_{crit} is a monotonically increasing function of radius, higher overall angular momentum will lead to: (i) a short quiescent interval, and (ii) a smaller circularization radius for the bulk of the innermost matter within the centrifugally supported disk, $r_{\text{circ}}[J(r_2)]$. Conversely, when the angular momentum normalization is low, the quiescence period will be longer, and the circularization radius for the majority of the innermost material will be greater. If the evolution of the late-time disk is driven by the viscous transport of angular momentum, the corresponding viscous time scale and the duration of the associated accretion episode will scale essentially with the initial disk radius. Thus, a longer quiescent period will be followed by a longer period of disk activity. The crucial point is that a lower global angular momentum normalization will place the bulk of the initial accreting matter capable of forming a centrifugally supported disk at a larger circularization radius. There is in addition an effective upper limit for this radius if the gas is to release its binding energy effectively, because if it is too large, the density and temperature will not be sufficient for neutrino cooling to operate.

As a final point, we may add that just as not all LGRBs exhibit this behavior, likewise it is clear from this work that not all progenitors are capable of producing the state transitions presented here. In fact, Perna & MacFadyen (2010) have recently argued that the lack of flaring activity in most LGRBs on long time scales is a signature of complete mixing in the progenitor, which is fully in agreement with the line of argument presented here. Once the deposition of energy in the inner regions of the star has produced a relativistic jet capable of traversing the stellar envelope, further variability may be reproduced in the overall light curve (Zhang et al. 2003). Determining whether this can power precursor activity is another matter, requiring the initial episode of accretion to create a low density polar funnel in the star, which remains to be addressed.

We thank S.E. Woosley and A. Heger for making their pre-SN models available. Part of this work was carried out during visits to the University of California, Santa Cruz whose hospitality is gratefully acknowledged. This work was supported in part by CONACyT-83254 (DLC, WL), DGAPA-UNAM-IN-113007 (DLC, WL), the David and Lucile Packard Foundation (ER) and UCMEXUS (ER and WL). DLC acknowledges support through a CONACyT graduate scholarship and a DGAPA-UNAM postdoctoral fellowship. We thank the referee for constructive criticism which helped improve the original version of the manuscript.

REFERENCES

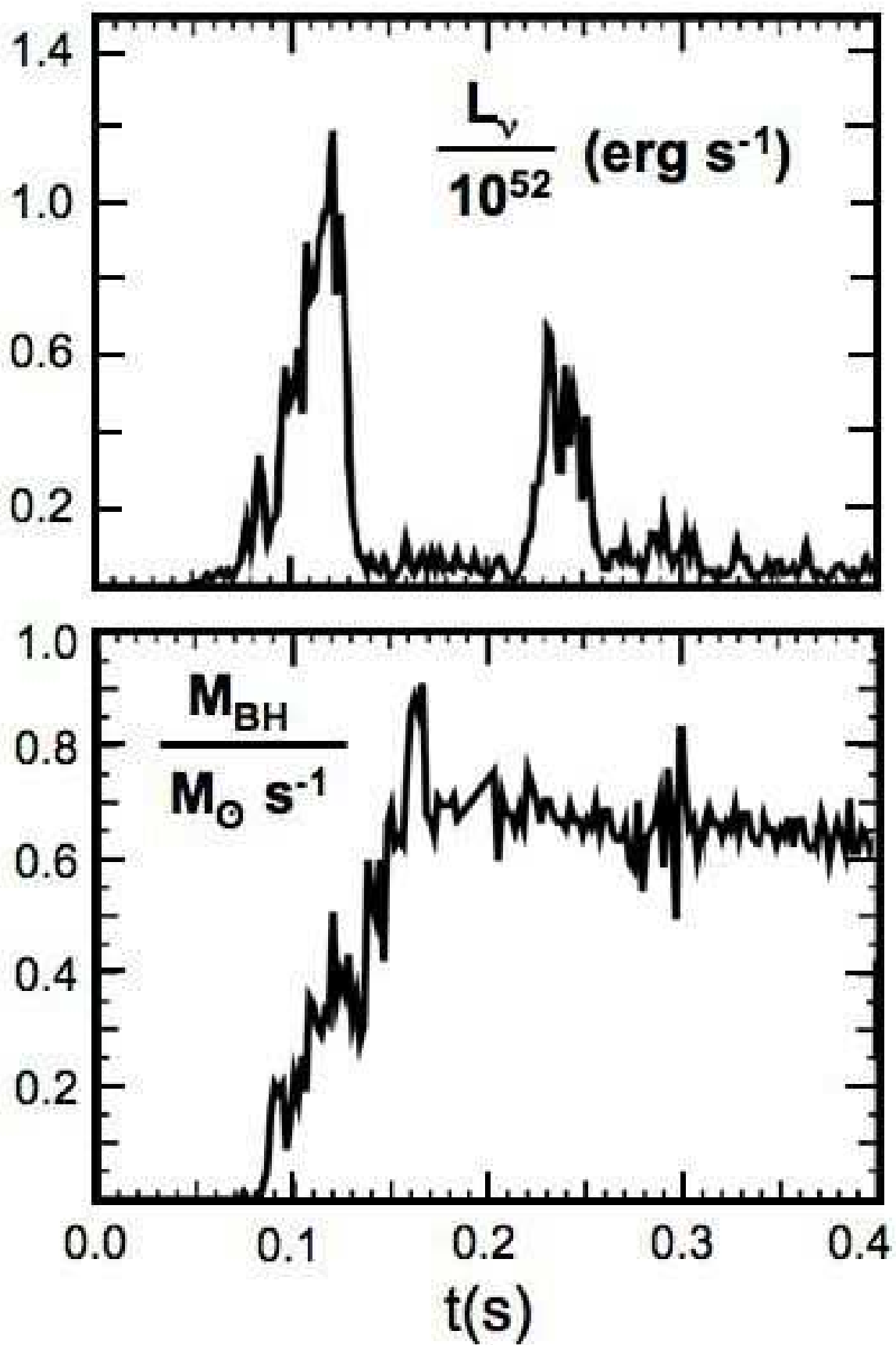
- Abramowicz, M. A., Calvani, M. & Nobili, L. 1983, *Nature*, 302, 597
- Aloy, M. A., Müller, E., Ibáñez, J. M., Martí, J. M., & MacFadyen, A. 2000, *ApJ*, 531, L119
- Aloy, M.-A., Ibáñez, J.-M., Miralles, J.-A., & Urpin, V. 2002, *A&A*, 396, 693
- Beloborodov, A.M., 2003, *ApJ*, 588, 931
- Blinnikov, S.I., Dunina-Barkovskaya, N.V., & Nadyozhin, D.K., 1996, *ApJS*, 106, 171
- Di Matteo, T., Perna, R., & Narayan, R. 2002, *ApJ*, 579, 706
- Fruchter, A.S. et al., 2006, *Nature*, 441, 463
- Fujimoto, S.-i., et al. 2006, *ApJ*, 644, 1040
- Gehrels, N., Ramirez-Ruiz, E. & Fox, D.B. 2009, *ARA&A*, 47, 567
- Heger, A., et al. 2000, *ApJ*, 528, 368
- Heger, A., Woosley, S.E., Spruit, H.C. 2005, *ApJ*, 626, 350
- Illarionov, A.F. & Beloborodov, A.M. 2001, *MNRAS*, 323, 159
- Itoh, N., et al. 1996, *ApJS*, 102, 411
- Janiuk, A., & Proga, D. 2008, *ApJ*, 675, 519
- Janiuk, A., Yuan, Y., Perna, R., & Di Matteo, T. 2007, *ApJ*, 664, 1011
- Kumar, P., Narayan, R., Johnson, J. L. 2008, *MNRAS*, 388, 1729
- Kumar, P., Narayan, R., Johnson, J. L. 2008, *Science*, 321, 376

- Langanke, K., & Marttínez-Pinedo Lattimer, G. 2001, *At. Data Nucl Data Tables*, 79, 1
- Lee, W. H., & Ramirez-Ruiz, E. 2006, *ApJ*, 641, 961
- Lee, W. H., Ramirez-Ruiz, & E., Page, D. 2005, *ApJ*, 632, 421
- Lindner, C. C., Milosavljević, M., Couch, S. M., & Kumar, P. 2010, *ApJ*, 713, 800
- López-Cámara, D., Lee, W. H., & Ramirez-Ruiz, E. 2009, *ApJ*, 692, 804, Paper I
- MacFadyen, A. I., & Woosley, S. E. 1999, *ApJ*, 524, 262
- MacFadyen, A. I., Woosley, S. E., & Heger, A. 2001, *ApJ*, 550, 410
- Nagataki, S., Takahashi, R., Mizuta, A., Takiwaki, T. 2007, *ApJ*, 659, 512
- Narayan, R., Piran, T., & Kumar, P. 2001, *ApJ*, 557, 949
- Paczynski, B., & Wiita, P. J. 1980, *A&A*, 88, 23
- Perna, R. & MacFadyen, A. 2010, *ApJ* 710, L103
- Popham, R., & Narayan, R. 1995, *ApJ*, 442, 337
- Popham, R., Woosley, S. E., & Fryer, C. 1999, *ApJ*, 518, 356
- Prochaska, J.X., Sheffer, Y., Perley, D. A., Bloom, J. S., Lopez, L. A., Dessauges-Zavadsky, M., Chen, H.-W., Filippenko, A. V., Ganeshalingam, M., Li, W., Miller, A. A., Starr, D., 2009, *ApJ*, 691, L27
- Proga, D., & Begelman M. C. 2003, *ApJ*, 582, 69
- Proga, D., MacFadyen, A. I., Armitage, P. J., & Begelman, M. C. 2003, *ApJ*, 599, L5
- Ramirez-Ruiz, E. & Merloni, A. 2001, *MNRAS*, 320, L25
- Ramirez-Ruiz, E., Merloni, A., & Rees, M. J. 2001, *MNRAS*, 324, 1147
- Ramirez-Ruiz, E., Celotti, A., Rees, M. J. 2002, *MNRAS*, 337, 1349
- Shakura, N. I., & Sunyaev, R. A. 1973, *A&A*, 24, 337
- Spruit, H.C. 2002, *A&A*, 381, 923
- Woosley, S.E., Bloom, J.S. 2006, *ARA&A*, 44, 507
- Woosley S. E., & Heger A. 2006, *ApJ*, 637, 914, WH06

Yoon, S.C., Langer, N., 2005, *A&A*, 443, 643

Zalamea, I., Beloborodov, A.M. 2009, *MNRAS*, 398, 2005

Zhang, W., Woosley, S. E., & MacFadyen, A. I. 2003, *ApJ*, 586, 356



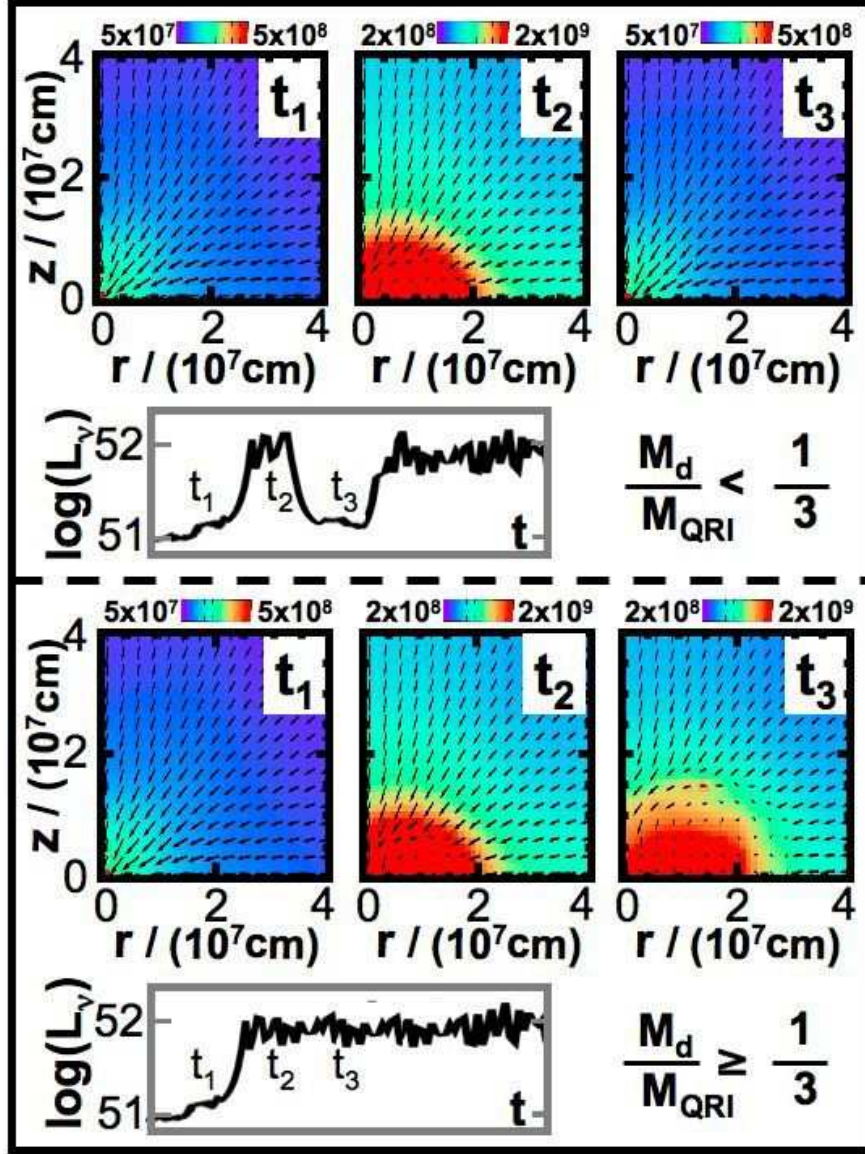


Fig. 3.— Density (in g cm^{-3}) and velocity field showing the flow morphology during the collapse in the stellar core. The snapshots, at $t_1 \leq t_2 \leq t_3$, are taken from simulations of model 16TI of WH06 for varying normalization factors in the radial distribution of specific angular momentum. Two possible evolutionary pathways are indicated. (a) Top: When $\mu = M_d/M_{\text{QRI}} < 1/3$, the initial QRI (t_1) is followed by the formation (t_2), destruction (t_3) and re-emergence of a centrifugal accretion disk. (b) Bottom: When $\mu \geq 1/3$, once a disk of mass M_d forms, it persists throughout the evolution as a coherent structure, surviving the infall of a low-angular momentum shell of mass M_{QRI} unperturbed. The transitions are reflected in the neutrino luminosity.

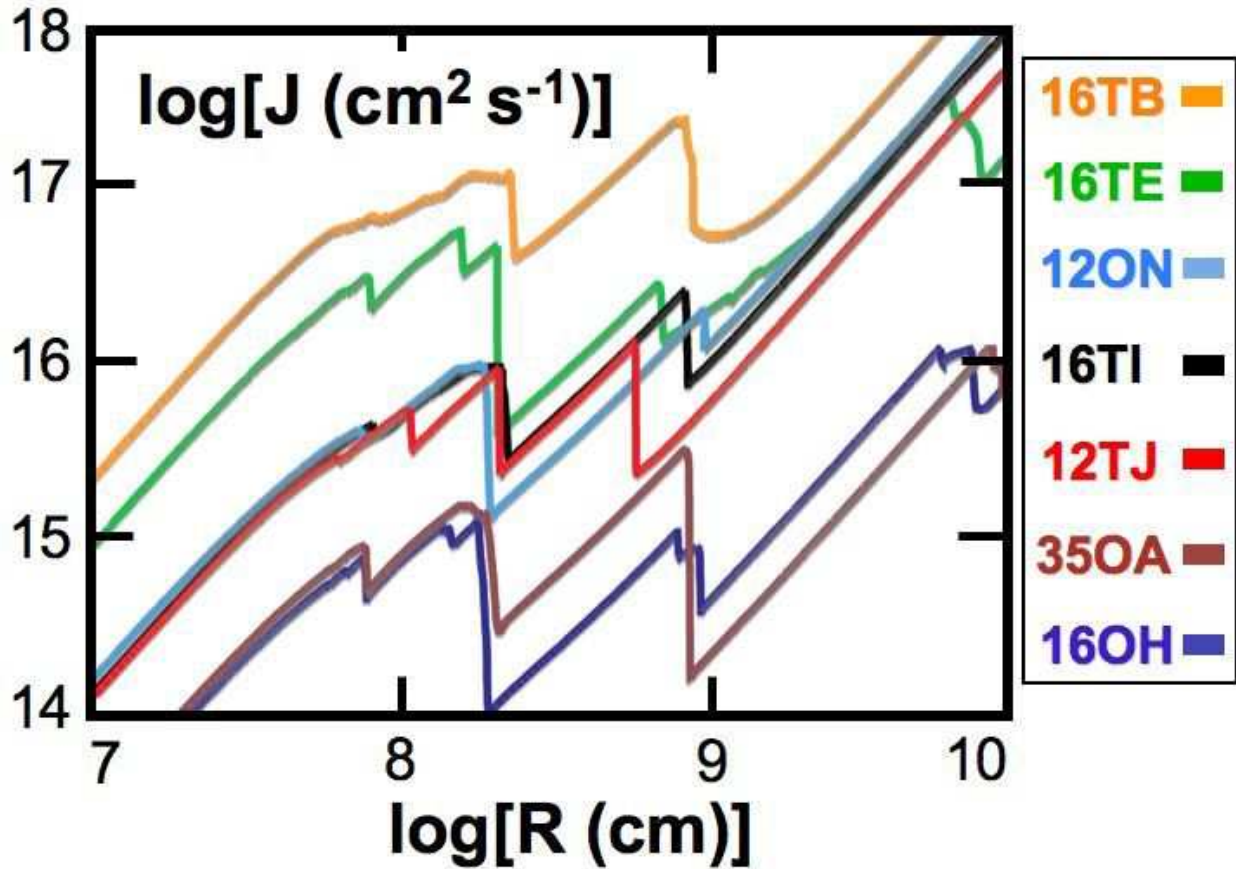


Fig. 4.— Distributions of specific angular momentum versus radius for representative pre-SN evolutionary models, taken from WH06. The initial rise at low radii is followed by a sharp drop, secondary increase and fall, and outer increase into the stellar envelope. Note the form similarity and the relative normalization differences, which is due to assumed metallicity, mass loss and magnetic field effects (see Table 1 for model parameters).

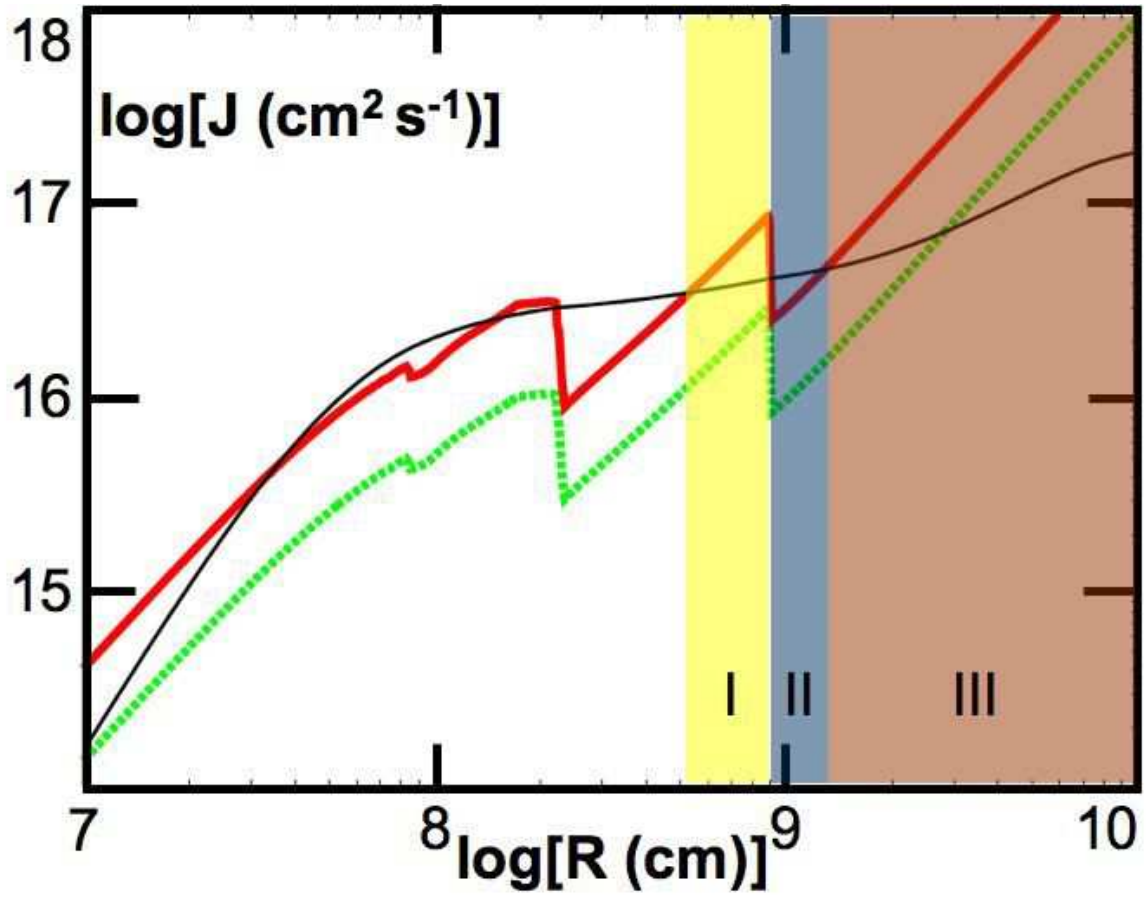


Fig. 5.— Radial distribution of angular momentum for model 16TI of WH06, $J_{16\text{TI}}(R)$ (green dotted line) and critical curve for the formation of a centrifugal barrier J_{crit} (thin black solid line) around the central Schwarzschild black hole with $M(R)$. The thick red line shows $f \times J(R)_{16\text{TI}}$ with $f = 2$.

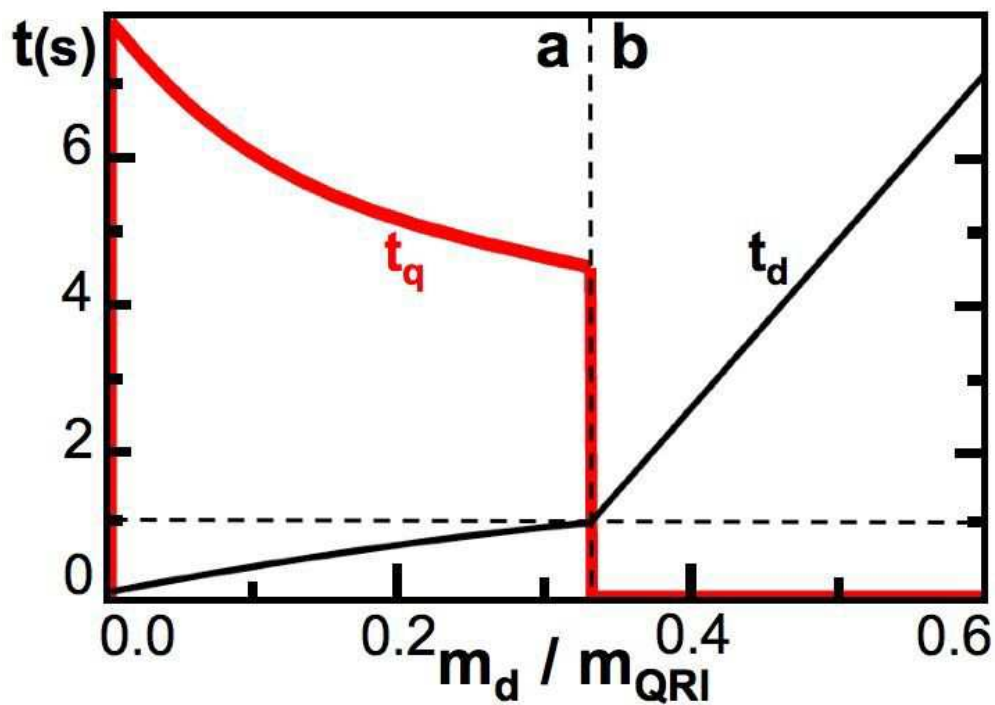


Fig. 6.— Quiescent period, t_q (red line) and initial disk activity, t_d (black line) episodes as a function of the high angular momentum disk to low angular momentum shell mass ratio, $\mu = M_d/M_{\text{sh}}$. If $\mu \leq 1/3$, $t_q + t_d$ varies slowly, while for $\mu \geq 1/3$ the quiescent episode abruptly disappears and $t_q = 0$. The dashed horizontal line approximately indicates the jet crossing time, t_{cross} , through the stellar envelope. In this case t_q is few seconds long, but can be significantly longer depending on the progenitor’s rotation.

Table 2: Model evolution time scales. Events with quiescent periods.

Model	$t_{\text{delay}}[s]$ ^a	$t_{\text{d}}[s]$	$t_{\text{q}}[s]$	$t_{\text{cross}}[s]$	f
16TB	0.5	2.3	9.6	1.8	0.6
16TE	1.3	0.9	3.0	1.8	2.0
12ON	3.5	0.6	1.6	1.5	1.9
16TI	2.3	1.1	4.2	1.0	2.0
12TJ	0.7	0.7	4.1	1.9	3.9
35OA	0.5	2.4	12.6	1.5	80
16OH	0.4	2.1	1.4	2.0	39

^aDelay between onset of collapse and initial rise in L_{ν} .